Orbital Order and Spin Nematicity in the Tetragonal Phase of Electron-doped Iron-Pnictides $NaFe_{1-x}Co_xAs$

R. Zhou,[1] L. Y. Xing,[1] X. C. Wang,[1] C. Q. Jin,[1] and Guo-qing Zheng[1,2]

[1]*Beijing National Laboratory for Condensed Matter Physics, Institute of Physics, Chinese Academy of Sciences, Beijing 100190, China*

[2]*Department of Physics, Okayama University, Okayama 700-8530, Japan*

(Dated: January 21, 2016)

arXiv:1601.05293v1 [cond-mat.supr-con] 20 Jan 2016

Abstract

In copper-oxide and iron-based high temperature (high-T_c) superconductors, many physical properties exhibit in-plane anisotropy, which is believed to be caused by a rotational symmetry-breaking nematic order, whose origin and its relationship to superconductivity remain elusive. In many iron-pnictides, a tetragonal-to-orthorhombic structural transition temperature T_s coincides with the magnetic transition temperature T_N, making the orbital and spin degrees of freedom highly entangled. NaFeAs is a system where $T_s = 54$ K is well separated from $T_N = 42$ K, which helps simplify the experimental situation. Here we report nuclear magnetic resonance (NMR) measurements on $NaFe_{1-x}Co_xAs$ ($0 \leq x \leq 0.042$) that revealed orbital and spin nematicity occurring at a temperature T^* far above T_s in the tetragonal phase. We show that the NMR spectra splitting and its evolution can be explained by an incommensurate orbital order that sets in below T^* and becomes commensurate below T_s, which brings about the observed spin nematicity.

Understanding the normal state out of which high-T_c superconductivity (SC) develops is an important task in condensed-matter physics. In copper-oxide high-temperature superconductors, the normal state deviates from the conventional state described by Landau Fermi liquid theory. In particular, below a certain temperature T^*, a so-called pseudogap state emerges, breaking the rotation symmetry of the underling lattices [1, 2]. In iron-pnictide or iron-selenide high-T_c superconductors, many physical properties in the normal state also show strong anisotropy (nematicity), breaking the four-fold rotation (C4) symmetry [3–5]. For example, in the parent Fe-pnictide $BaFe_2As_2$, electronically-driven nematicity was discovered in the in-plane resistivity below a tetragonal-to-orthorhombic structural transition temperature T_s [3, 6]. Soon after the transport measurements, angle resolved photo-emission spectroscopy (ARPES) found that the degeneracy of the Fe-3d_{xz} and 3d_{yz} orbitals is lifted [4]. Later on, nematicity was also found in other properties ranging from magneto-elastic property in chemically-pressurized $BaFe_2As_2$ [5], to spin dynamics in carrier-doped $BaFe_2As_2$ [7], and to local electronic structure around defects even above T_s [8, 9]. Theoretically, both spin [10] and orbital origin [11–14] have been proposed for the cause of the experimentally-observed nematicity. In the $BaFe_2As_2$ family, however, antiferromagnetism (AF) sets in simultaneously at T_s or slightly below [15]. As a result, it is unclear whether the transition is driven by spin degree of freedom [10] or by orbital degree of freedom [11–14]. Neither is it clear whether the nematicity is caused by a static [5] or a fluctuating order [7]. Therefore, identifying the origin of the nematicity has become an urgent issue, since it is believed that the interaction leading to such a nematicity may also be responsible for the high-T_c superconductivity[16, 17].

NaFeAs is a unique system where T_s = 54 K is well above T_N = 42 K. Only 2.7 percent of Co substituting for Fe gives rise to the maximum T_c = 21 K [18], which makes the system a clean one with much less doping-induced disorder than other systems. In this Communication, we report evidence pointing toward orbital order at a temperature T^* (as high as 90 K) that is far above T_s in $NaFe_{1-x}Co_xAs$ by ^{75}As and ^{23}Na NMR spectroscopy. We further revealed a spin nematicity in this system by the spin-lattice relaxation rate ($1/T_1$) measurements, and show that it can be understood as a direct consequence of the orbital order.

The single crystals of $NaFe_{1-x}Co_xAs$ used for the measurements were grown by the self-flux method[8]. In order to prevent sample degradation, The samples were covered by Stycast 1266® in a glove box filled with high-purity Ar gas[19]. The typical sample size is 3mm×3mm×0.1mm. The Co content x was determined by energy-dispersive x-ray spectroscopy. The T_c was determined by DC susceptibility measured by a SQUID device. The NMR spectra were obtained by integrating

the spin echo as a function of frequency at H_0 = 11.998 T. The T_1 was measured by using the saturation-recovery method, and determined by a good fitting to the theoretical curve [20].

The ^{75}As or ^{23}Na nucleus with spin I = 3/2 has a nuclear quadrupole moment Q that couples to the electric field gradient (EFG) $V_{\alpha\alpha}$ ($\alpha = x, y, z$), relating to the NQR frequency tensors $\nu_\alpha = \frac{eQ}{4I(2I-1)}V_{\alpha\alpha}$. Therefore, both ^{75}As- and ^{23}Na-NMR are good probes for a structural phase transition as shown in NaFeAs where the principal axes are along the crystal axes [21]. In addition, the As site is very close to the Fe plane so that the As-p and Fe-d orbitals strongly hybridize, which makes ^{75}As NMR also a sensitive and unique probe for detecting an orbital order since a disparate occupation in As-p orbitals will produce an asymmetric EFG.

When a magnetic field H_0 is applied along i-axis ($i = a$ or b), the NMR resonance frequency f is expressed by [22]

$$f_{m\leftrightarrow m-1,i} = \gamma_N H_0 (1 + K_i) + \frac{1}{2}\nu_c \left(m - \frac{1}{2}\right)(n_i \cdot \eta - 1) + a_m \delta f_i \tag{1}$$

, where K_i is the Knight shift, m = 3/2, 1/2 and -1/2, and $n_i = \mp 1$. $\eta \equiv \frac{|V_{xx}-V_{yy}|}{V_{zz}} = \left|\frac{\nu_a-\nu_b}{\nu_a+\nu_b}\right|$ is the asymmetry parameter of the EFG, which measures a nematicity in the ab-plane. Finally, $a_m \delta f_i$ is the second-order quadrupolar shift when H_0 is applied parallel to i-axis, and is given as,

$$\begin{aligned} \delta f_a &= \frac{(\nu_b - \nu_c)^2}{12(1 + K_a)\gamma_N H_0} = \frac{3\nu_c^2}{16(1 + K_a)\gamma_N H_0}\left(1 - \frac{\eta}{3}\right)^2 \\ \delta f_b &= \frac{(\nu_a - \nu_c)^2}{12(1 + K_b)\gamma_N H_0} = \frac{3\nu_c^2}{16(1 + K_b)\gamma_N H_0}\left(1 + \frac{\eta}{3}\right)^2 \end{aligned} \tag{2}$$

This correction only needs to be considered for the central transition (m=1/2) line, so $a_{1/2}$ = 1 and $a_{3/2} = a_{-1/2}$ =0. For a material with C4 rotation symmetry, η = 0. However, $\eta > 0$ if C4 symmetry is broken. Therefore, for a twined single crystal with C2 symmetry, the field configurations of $H_0 \parallel a$-axis and $H_0 \parallel b$-axis will give a different $f_{m\leftrightarrow m-1,i}$, leading to a splitting of both satellite and central peaks.

Figure 1 shows the evolution of the NMR spectra in NaFeAs. At high temperature (T), only one central transition and a pair of satellites are observed. Below T^* = 90 K, a broadening of both central and satellite lines was seen in the ^{75}As-NMR spectra, but not in the ^{23}Na-NMR lines. With further decreasing T, all the ^{75}As-NMR lines become narrower below T_s, and a clear splitting is observed. Same is true for ^{23}Na-NMR lines below T_s. Note that T^* is much higher than the $T_s \sim$ 54 K confirmed by both previous neutron scattering measurement [23] and our resistivity data [19].

One apparent possibility for the ^{75}As-NMR lines broadening (splitting) is that there are some small local orthorhombic domains existing above T_s formed by tiny uniaxial pressure from disor-

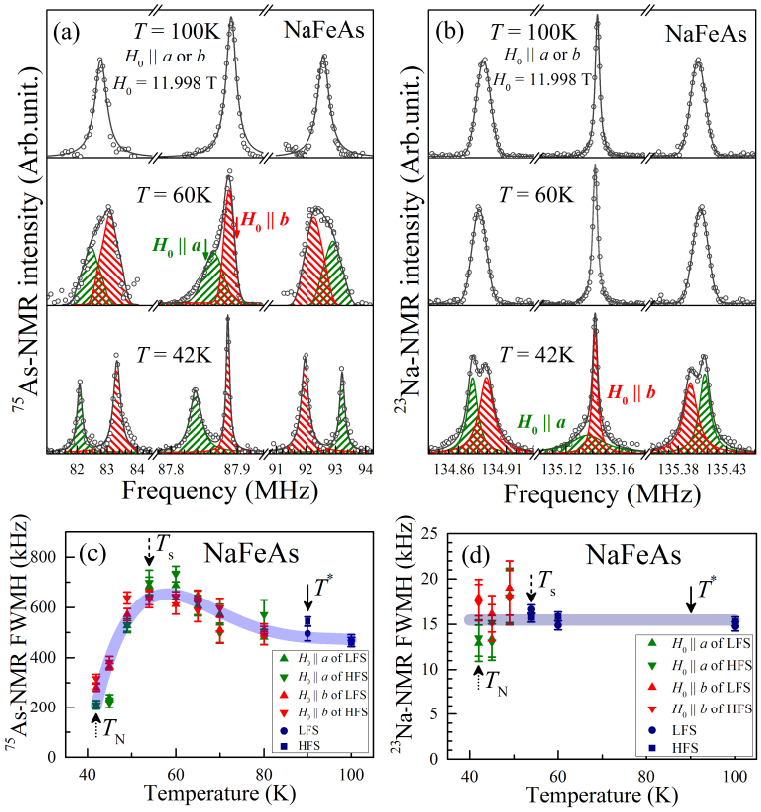

FIG. 1: **(a-b)** ^{75}As- and ^{23}Na-NMR spectra. The three peaks at T = 100 K respectively correspond to the low frequency satellite (LFS), central transition and high frequency satellite (HFS). The middle panel in **(a)** shows the simulation of 2D-incommensurate orbital order model for T = 60 K spectra. Green (red) shadow area represents the transitions with H_0 || a-axis (b-axis). The green and red arrows show the positions at which $1/T_{1a}$ and $1/T_{1b}$ was measured, respectively. At T = 100 K, $1/T_1$ measured at low- and high-frequency tails gives rise to the same value. **(c-d)**, T-dependence of the full width at half maximum (FWHM) of each peak.

ders [9, 24] or uniaxial strains due to epoxy encapsulation. However, this can be ruled out since ^{23}Na-NMR spectra do not change below T^* and there is no angular dependence of T^* [19]. The other is that orbitals order in the real tetragonal phase. In this case, the origin of EFG asymmetry is the Fe orbital order parameter Δ. For example, for the orbital splitting found in ARPES [4], one can write $\Delta \propto (n_{xz}^{3d} - n_{yz}^{3d})$, where n is the electron density. It will produce a population disparity between As-4p_x and 4p_y, $(n_x^{4p} - n_y^{4p})$, through Fe-As orbital hybridization. Such disparity was explained by electronic mechanism [10–14], as well as by local-density approximations calculation [25]. At the moment, we cannot rule out other form of Δ that can produce a finite $(n_x^{4p} - n_y^{4p})$. The

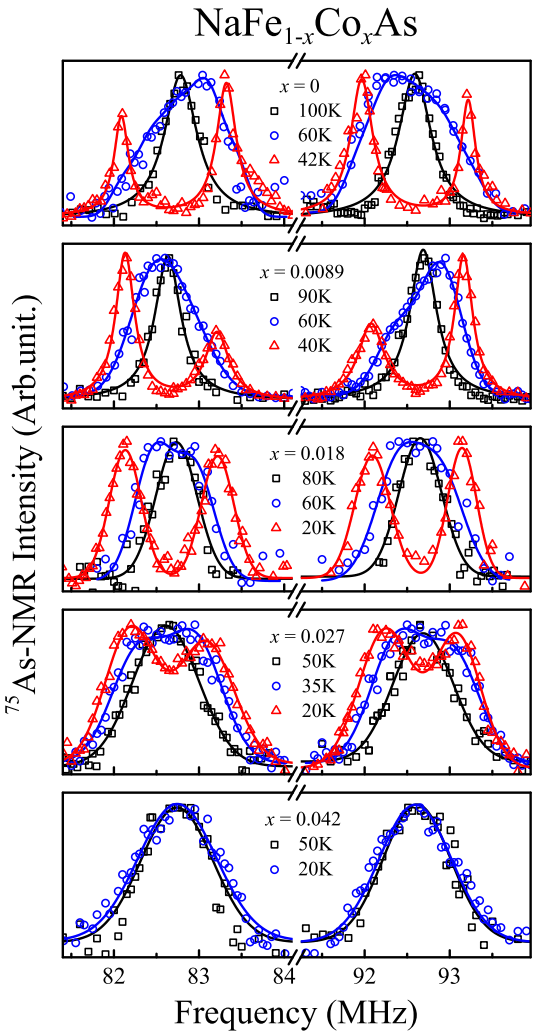

FIG. 2: T-evolution of the ^{75}As-NMR satellite peaks. For $x = 0$, 0.0089, 0.018 and 0.027, the peaks are broadened below T^*, and split below T_s. For $x = 0.042$, however, no clear change in the spectrum is detected down to $T = 20$ K.

As-NQR frequency tensor $\nu_{x,y,z}$ is related to $n^{4p}_{x,y,z}$ as [26]

$$\begin{bmatrix} \nu_x \\ \nu_y \\ \nu_z \end{bmatrix} = \nu_0 \begin{bmatrix} n_x^{4p} - \frac{n_y^{4p}+n_z^{4p}}{2} \\ n_y^{4p} - \frac{n_x^{4p}+n_z^{4p}}{2} \\ n_z^{4p} - \frac{n_x^{4p}+n_y^{4p}}{2} \end{bmatrix} \quad (3)$$

where ν_0 is the NQR frequency when there is one electron (hole) in each $4p$-orbital. It follows that $\left|\nu_x - \nu_y\right| = \frac{3\nu_0}{2}\left|n_x^{4p} - n_y^{4p}\right|$, therefore $\eta_{As} \propto \left|n_x^{4p} - n_y^{4p}\right| \propto \Delta$.

Below we show that an incommensurate orbital order in the tetragonal phase, which becomes commensurate below T_s, can consistently account for the observed results. The observed behavior

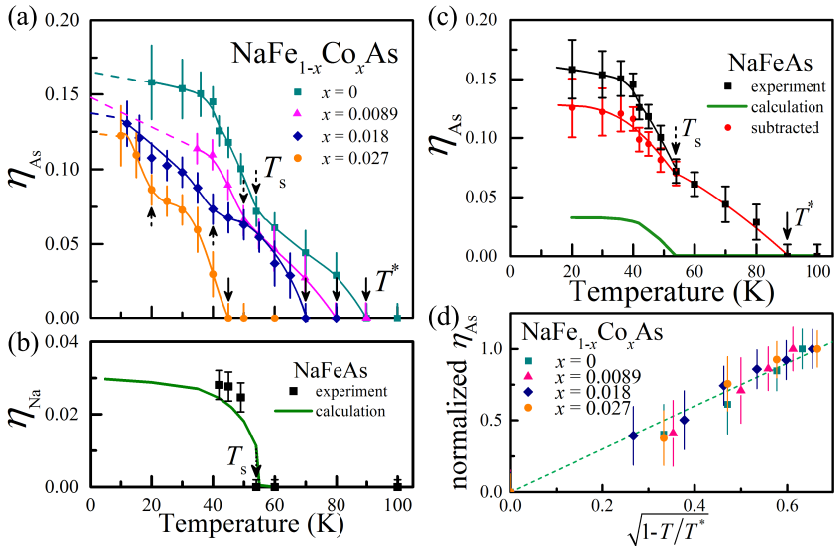

FIG. 3: The evolution of the EFG asymmetry parameter η. **(a)** T-dependence of η_{As} for various x. The solid and dotted arrows indicate T^* and T_{s}, respectively. **(b)** T-dependence of η_{Na} for x=0. The green curve is the contribution due to the structure change obtained by all-electron full-potential linear augmented plane wave method [27, 28], by using the lattice parameter from neutron scattering [23] and X-ray diffraction [29]. **(c)** Experimental, calculated and the subtracted data of η_{As} for x=0. **(d)** η_{As} normalized by its value at T_{s} against $\sqrt{1-T/T^*}$ for various x.

is very similar to the crossover of commensurate to incommensurate antiferromagnetic order in NaFeAs[21]. Generally speaking, in a commensurate density-wave state, the NMR line reflects the small number of physically non-equivalent nuclear sites in the unit cell so that the linewidth is small. In an incommensurate state, however, since the translational periodicity is lost, the number of non-equivalent nuclear sites is larger which gives rise to a larger linewidth [30]. In the present case, A modulation due to orbital order will cause an additional term in the resonance frequency at As site (x, y). Let this term be a cosine function as $\left[\cos\left(\frac{2\pi}{a}q_x \cdot x + \theta_x\right) + \cos\left(\frac{2\pi}{b}q_y \cdot y + \theta_y\right)\right]$, where q_x and q_y are the two-dimensional (2D) wave vectors and $\theta_{x,y}$ is the phase. Then, for commensurate order, the additional term becomes $\left[\cos\theta_x + \cos\theta_y\right]$, which is site-independent. For incommensurate order, however, this term is site-dependent, which leads to a broadening of the spectrum. By convoluting with a Gaussian function [19], we can reproduce the spectra as shown in Fig. 1 (a). In passing,we note that T^*=90 K for x=0 is consistent with the temperature below which scanning tunneling microscope found local electronic nematicity by quasiparticle interference [8].

Below T_{s}, the ^{75}As-NMR spectra become narrower and each peak is well resolved. Moreover,

no NMR intensity loss is observed below T_s ord T^*[19]. All these imply that all the As sites have the same environment. That is, the orbital order becomes commensurate. The doping dependence of the spectra is shown in Fig. 2. As for x=0, a peak splitting was also found above T_s for x = 0.0089, 0.018 and 0.027, which get well resolved at T_s. For x = 0.042, however, no change of the spectra was found down to T = 20 K.

More quantitative data are shown in Fig. 3 where the evolution of η is demonstrated. The η_{As} develops continuously below T^*, showing a saturation tendency approaching T_s. In contrast, η_{Na} shows up only below T_s and the absolute value is much smaller than η_{As}, indicating that it is purely due to the structural transition. There are two contributions to the observed η, $\eta = \eta_{lattice} + \eta_{orbital}$, where $\eta_{lattice}$ is due to surrounding lattice and $\eta_{orbital}$ is due to orbital order on Fe site. By the first principle calculation, we find that the observed η_{Na} is well explained by the change in $\eta_{lattice}$; the discrepancy is about 10%. Another remarkable feature of η_{As} is that it increases steeply again below T_s, which cannot be accounted by the calculated $\eta_{lattice}$. The red circles in Fig. 3 (d) is the net increase after subtracting the effect due to the lattice change. A clear kink can be seen at T_s, which is true even after multiplying the calculated result by a factor of 1.1~1.15. The increase is consistent with the incommensurate-to-commensurate transition. In the incommensurate state, $\left|n_x^{4p} - n_y^{4p}\right|$ is inhomogeneous and η_{As} probes the averaged $\left|n_x^{4p} - n_y^{4p}\right|$. In the commensurate state, η_{As} measures the homogeneous $\left|n_x^{4p} - n_y^{4p}\right|$, which can be larger [19].

Finally, it is worthwhile pointing out that η_{As} shows a linear relationship with $\sqrt{1 - T/T^*}$ for all samples in the vicinity of T^*, as shown in Fig. 3 (d), suggesting that the nematic order undergoes a Landau-type-like second-order phase transition. The T^* and T_s results obtained by NMR are summarized in the phase diagram shown in Fig. 4.

Next we turn to the spin dynamics of this system. which was also clearly seen below T^* in $1/T_1$. Figure 5 (a) shows the $1/T_1$ results for x = 0, 0.0089 and 0.018. Below T^*, $1/T_1$ measured at the positions corresponding to $H_0 \parallel [100]_o$ (a-axis) and $H_0 \parallel [010]_o$ (b-axis) shows opposite T-dependence. Here we assign the direction with larger NQR frequency tensor to the a-axis. Figure 5 (b) shows the ratio of the two T_1. As in $Ba(Fe_{1-x}[Ni,Co]_x)_2As_2$ [15, 31], $1/T_1$ arises from the antiferromagnetic spin fluctuations and the contribution due to the intra-band (DOS at the Fermi level), but the former is dominant [19]. We show below that the anisotropy of $1/T_1$ is a natural consequence of the orbital order.

The magnetic order on the Fe atoms below T_N is of stripe type with ordering vectors $Q_X = (\pi,0)$ [23]. Above T_N, however, magnetic fluctuations from $Q_Y = (0,\pi)$ also exist and have the equal

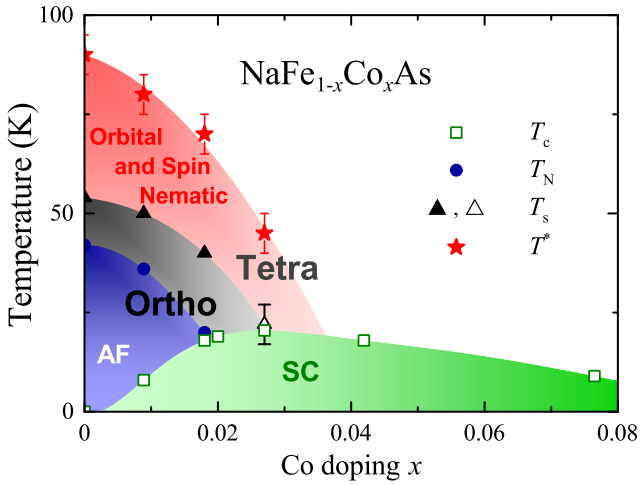

FIG. 4: The obtained phase diagram. For x <0.027, T_s agrees well with that from resistivity [19]. For x = 0.027, the T_s coincides with T_c so that direct comparison with resistivity is unavailable. To distinguish with other compositions, the data point is represented by an open triangle. Ortho and Tetra represent the orthorhombic and tetragonal phase, respectively.

amplitude as those from Q_X. Since As sits above or below the center of the square formed by four irons, $1/T_1$ of ^{75}As along the orthorhombic a-direction or b-direction sees antiferromagnetic spin fluctuations from both Q_X and Q_Y as follows [32]

$$\left(\frac{1}{T_1}\right)_a^{Q_X} \propto A^2\chi''_a \qquad \left(\frac{1}{T_1}\right)_b^{Q_X} \propto A^2(\chi''_a + \chi''_c) \tag{4}$$

and

$$\left(\frac{1}{T_1}\right)_a^{Q_Y} \propto A^2(\chi''_b + \chi''_c) \qquad \left(\frac{1}{T_1}\right)_b^{Q_Y} \propto A^2\chi''_b \tag{5}$$

Here A is the hyperfine coupling constant and χ''_j $(j = a, b, c)$ is the imaginary part of the staggered susceptibility. The measured $(1/T_1)_i$ $(i = a, b)$ can then be written as

$$\left(\frac{1}{T_1}\right)_i = N_X\left(\frac{1}{T_1}\right)_i^{Q_X} + N_Y\left(\frac{1}{T_1}\right)_i^{Q_Y} \tag{6}$$

where N_X (N_Y) is the relative weight of contribution from Q_X (Q_Y), with $N_X + N_Y = 1$. It then follows

$$\frac{(1/T_1)_b}{(1/T_1)_a} = \frac{\chi''_c + \chi''_a + \frac{N_Y}{N_X}\chi''_b}{\chi''_a + \frac{N_Y}{N_X}(\chi''_b + \chi''_c)} \tag{7}$$

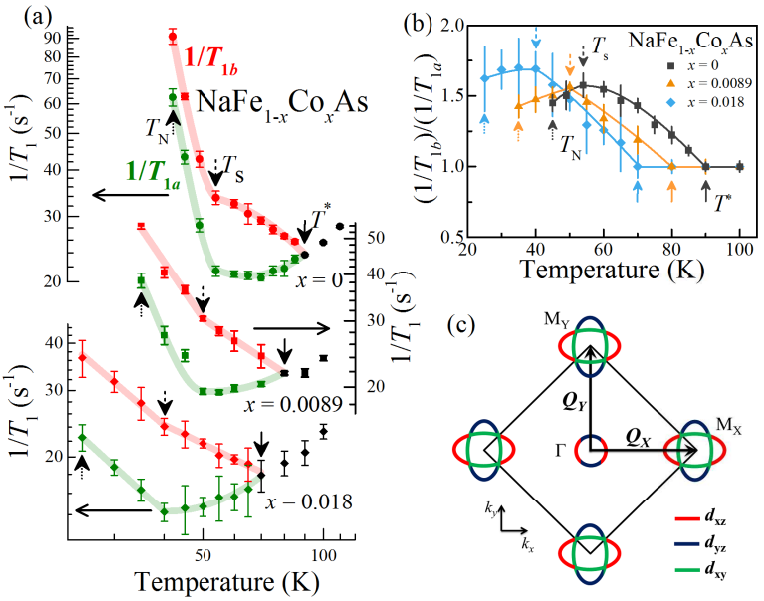

FIG. 5: **(a)** T-dependence of $1/T_1$ for various x. **(b)** T dependence of $1/T_1$ ratio. Solid, dashed and dotted arrows indicate T^*, T_s and T_c, respectively. **(c)** Schematics of the Fermi surface (FS) obtained by ARPES [35] and the spin fluctuations wave vectors. The outer FS centered at Γ is omitted here for clarity. The color represents the Fe-3$d_{xz,yz,xy}$ orbital character.

which measures a change in the ratio $\frac{N_Y}{N_X}$. The $1/T_1$ ratio will always be a unity as long as $N_X = N_Y$. On the other hand, in the limit of $N_X \sim 1$ and $N_Y \sim 0$, the ratio will be 2, since polarized inelastic neutron scattering found that the anisotropy in the low-energy spin excitations above T_s is small, if any [33].

As seen in Fig. 5 (b), the observed ratio $\frac{(1/T_1)_b}{(1/T_1)_a}$ increases below T^*, indicating that N_X increases and N_Y decreases. These results are a natural consequence of orbital order with the occupation of Fe-3d_{xz} becoming larger than Fe-3d_{yz} which changes the FS nesting condition so that spin fluctuations with Q_X becomes dominant [34]. This is because Q_X connects the Fermi pocket centered at Γ = (0,0) with that centered at $M_X = (\pi,0)$ consisting of d_{xz} orbital, and Q_Y connects the Γ Fermi pocket with that centered at $M_Y = (0, \pi)$ consisting of d_{yz} orbital (see Fig. 5 (c)). Finally, we note that an anomaly is found at T_s in $1/T_1$ of both directions, which is consistent with a change in the character of orbital order, but the detailed analysis of the anomaly and theoretical explanation are a topic of future investigation.

Previously, electronic nematicity was found in $BaFe_2As_2$ [4, 5, 15] and FeSe [36–40] systems, but it occurs right at T_s. Above T_s, only fluctuations were observed [41, 42]. In Ni-doped

$BaFe_2As_2$, although anisotropy was found in the spin susceptibility above T_s, the system was under a uni-axial pressure and it was attributed to a fluctuating order [7]. By contrast, no external driving force was applied in the present case, thus the observation of a static order at the time scale of 10^{-8} sec is unprecedented.

In summary, we have presented the systematic NMR measurements on single crystals of $NaFe_{1-x}Co_xAs$. The ^{75}As-spectra were broadened at T^* far above T_s and get well split below T_s. The EFG asymmetry parameter η emerges below T^* and increases abruptly below T_s. However, the ^{23}Na-NMR spectra showed no change until T_s. These results can be explained by an incommensurate orbital order formed in the tetragonal phase which becomes commensurate below T_s. A spin nematicity is also found below T^*, which can be understood as a direct consequence of the orbital order.

Acknowledgments

We thank T. Xiang for helpful discussion and comments, M.-H. Julien and S. Onari for a critical reading of the manuscript, S. Maeda and T. Oguchi for advice and help in the EFG calculation, Z. Li and J. Yang for assistance in some of the measurements. This work was partially supported by CAS Strategic Priority Research Program, No. XDB07020200 and by a 973 project National Basic Research Program of China, No. 2012CB821402.

[1] M. J. Lawler, K. Fujita, Jhinhwan Lee, A. R. Schmidt, Y. Kohsaka, Chung Koo Kim, H. Eisaki, S. Uchida, J. C. Davis, P. Sethna and Eun-Ah Kim, Intra-unit-cell electronic nematicity of the high-T_c copper-oxide pseudogap states. Nature **466**,347-351 (2010).

[2] R. Daou, J. Chang, David LeBoeuf, O. Cyr-Choinière, F. Laliberté, N. Doiron-Leyraud, B. J. Ramshaw, R. Liang, D. A. Bonn, W. N. Hardy and L. Taillefer, Broken rotational symmetry in the pseudogap phase of a high-T_c superconductor. Nature **463**, 519-522 (2010).

[3] J.-H. Chu, J. G. Analytis, K. De Greve, P. L McMahon, Z. Islam, Y. Yamamoto, and I. R. Fisher, In-Plane Resistivity Anisotropy in an Underdoped Iron Arsenide Superconductor. Science **329**, 824-826 (2010).

[4] M. Yi, D.H. Lu, J.-H. Chu, J. G. Analytis, A.P. Sorinia, A. F. Kemper, B. Moritz, S.-K. Mod, R. G. Moore , M. Hashimoto, W.-S. Lee, Z. Hussain, T. P. Devereaux, I. R. Fisher and Z.-X. Shen, Symmetry breaking orbital anisotropy on detwinned $Ba(Fe_{1-x}Co_x)_2As_2$ above the spin density wave transition. Proc. Nat. Acad. Sci. **108**, 6878-6883 (2011).

[5] S. Kasahara, H. J. Shi, K. Hashimoto, S. Tonegawa, Y. Mizukami, T. Shibauchi, K. Sugimoto, T. Fukuda, T. Terashima, Andriy H. Nevidomskyy and Y. Matsuda, Electronic nematicity above the structural and superconducting transition in $BaFe_2(As_{1-x}P_x)_2$. Nature **486**, 382-385 (2012).

[6] J.-H. Chu, H.-H. Kuo, J. G. Analytis and I. R. Fisher, Divergent nematic susceptibility in an iron arsenide superconductor. Science **337**, 710 (2012).

[7] X. Y. Lu , J. T. Park, R. Zhang, H. Q. Luo, A. H. Nevidomskyy, Q. M. Si, P. C. Dai, Nematic spin correlations in the tetragonal state of uniaxial-strained $BaFe_{2-x}Ni_xAs_2$. Science **345**, 657-660 (2014).

[8] E. P. Rosenthal, E. F. Andrade, C. J. Arguello, R. M. Fernandes, L. Y. Xing, X. C. Wang, C. Q. Jin, A. J. Millis and A. N. Pasupathy, Visualization of electron nematicity and unidirectional antiferroic fluctuations at high temperatures in NaFeAs. Nat. Phys. **10**, 225-232 (2014).

[9] T. Iye, M.-H. Julien, H. Mayaffre, M. Horvati, C. Berthier, K. Ishida, H. Ikeda, S. Kasahara, T. Shibauchi, and Y. Matsuda, Emergence of Orbital Nematicity in the Tetragonal Phase of $BaFe_2(As_{1-x}P_x)_2$. J. Phys. Soc. Jpn. **84**, 043705 (2015).

[10] R. M. Fernandes, A. V. Chubukov, J. Knolle, I. Eremin, and J. Schmalian, Preemptive nematic order, pseudogap, and orbital order in the iron pnictides. Phys. Rev. B **85**, 024534 (2012).

[11] W. Lv, F. Kruger, and P. Phillips, Orbital ordering and unfrustrated (π,0) magnetism from degenerate double exchange in the iron pnictides. Phys. Rev. B **82**, 045125 (2010).

[12] C.-C. Lee, W.-G. Yin, and W. Ku, Ferro-Orbital Order and Strong Magnetic Anisotropy in the Parent Compounds of Iron-Pnictide Superconductors. Phys. Rev. Lett. **103**, 267001 (2009).

[13] S. Onari, and H. Kontani, Self-consistent Vertex Correction Analysis for Iron-based Superconductors: Mechanism of Coulomb Interaction-Driven Orbital Fluctuations. Phys. Rev. Lett. **109**, 137001 (2012).

[14] H. Kontani, and Y. Yamakawa, Linear Response Theory for Shear Modulus C_{66} and Raman Quadrupole Susceptibility: Evidence for Nematic Orbital Fluctuations in Fe-based Superconductors. Phys. Rev. Lett. **113**, 047001 (2014).

[15] R. Zhou, Z. Li, J. Yang, D. L. Sun, C. T. Lin, and G.Q. Zheng, Quantum Criticality in electron-doped $BaFe_{2-x}Ni_xAs_2$. Nat. Commun. **4**, 2265 (2013).

[16] R. M. Fernandes, A. V. Chubukov, and J. Schmalian, What drives nematic order in iron-based super-

conductors? Nat. Phys. **10**, 97-104 (2014).

[17] J. Yang, R. Zhou, L. L. Wei, H. X. Yang, J. Q. Li, Z. X. Zhao, G. Q. Zheng, New Superconductivity Dome in $LaFeAsO_{1-x}F_x$ Accompanied by Structural Transition, Chinese Phys. Lett. **32**, 107401 (2015).

[18] D. R. Parker, M. J. Pitcher, P. J Baker, I. Franke, T. Lancaster, S. J. Blundell, S. J. Clarke, Structure, antiferromagnetism and superconductivity of the layered iron arsenide NaFeAs. Chem. Commun. **16**, 2189-2191 (2009).

[19] See supplemental materials for the details.

[20] A. Narath, Nuclear Spin-Lattice Relaxation in Hexagonal Transition Metals: Titanium. Phys. Rev. **162**, 320-332 (1967).

[21] K. Kitagawa, Y. Mezaki, K. Matsubayashi, Y. Uwatoko, and M. Takigawa, Crossover from Commensurate to Incommensurate Antiferromagnetism in Stoichiometric NaFeAs Revealed by Single-Crystal ^{23}Na, ^{75}As-NMR Experiments. J. Phys. Soc. Jpn. **80**, 033705 (2011).

[22] A. Abraham, Principles of Nuclear Magnetism Ch. 7 (Oxford Univ. Press, Oxford, 1961).

[23] S. Li, C. de la Cruz, Q. Huang, G. F. Chen, T.-L. Xia, J. L. Lou, N. L. Wang, abd P. C. Dai, Structural and magnetic phase transitions in $Na_{1-\delta}FeAs$. Phys. Rev. B **80**, 020504 (2009).

[24] Y. Inoue, Y. Yamakawa, and H. Kontani, Impurity-induced electronic nematic state and C_2-symmetric nanostructures in iron pnictide superconductors, Phys. Rev. B **85**, 224506 (2012)

[25] T. Shimojima, K. Ishizaka, Y. Ishida, N. Katayama, K. Ohgushi, T. Kiss, M. Okawa, T. Togashi, X.-Y. Wang, C.-T. Chen, S. Watanabe, R. Kadota, T. Oguchi, A. Chainani, and S. Shin, Orbital-Dependent Modifications of Electronic Structure across the Magnetostructural Transition in $BaFe_2As_2$. Phys. Rev. Lett. **104**, 057002 (2010).

[26] G. Q. Zheng, Y. Kitaoka, K. Ishida, and K. Asayama, Local hole distribution in the CuO_2 plane of high-T_c copper-oxides studied by Cu and oxygen NMR/NQR. J. Phys. Soc. Jpn. **64**, 2524 (1995).

[27] P. Blaha, K. Schwarz, and P. H. Dederichs, First-principles calculation of the electric-field gradient in hcp metals. Phys. Rev. B **37**, 2792 (1988).

[28] T. Oguchi, Electronic band structure and structural stability of LaBiPt. Phys. Rev. B **63**, 125115 (2001).

[29] D. R. Parker, M. J. P. Smith, T. Lancaster, A. J. Steele, I. Franke, P. J. Baker, F. L. Pratt, M. J. Pitcher, S. J. Blundell, and S. J. Clarke, Control of the Competition between a Magnetic Phase and a Superconducting Phase in Cobalt-Doped and Nickel-Doped NaFeAs Using Electron Count. Phys.

Rev. Lett. **104**, 057007 (2010).

[30] R. Blinc, and T. Apih, NMR in multidimensionally incommensurate and CDW systems, Prog. Nucl. Mag. Res. Spec. **41**, 49 (2002).

[31] F. L. Ning, K. Ahilan, T. Imai, A. S. Sefat, M. A. McGuire, B. C. Sales, D. Mandrus, P. Cheng, B. Shen, and H. H. Wen, Contrasting spin dynamics between underdoped and overdoped $Ba(Fe_{1-x}Co_x)_2As_2$. Phys. Rev. Lett. **104**, 037001 (2010).

[32] Z. Li, D. L. Sun, C. T. Lin, Y. H. Su, J. P. Hu and Guo-qing Zheng, Nodeless energy gaps of single-crystalline $Ba_{0.68}K_{0.32}Fe_2As_2$ as seen via ^{75}As NMR. Phys. Rev. B **83**, 140506 (2011).

[33] Y. Song, L. -P. Regnault, C. Zhang, G. Tan, S. V. Carr, S. Chi, A. D. Christianson, T. Xiang, and P. Dai, In-plane spin excitation anisotropy in the paramagnetic state of NaFeAs. Phys. Rev. B **88**, 134512 (2013).

[34] Y. Su, C. Zhang, and T. Li, Influence of orbital nematic order on spin responses in Fe-based superconductors. arXiv:1412.0210v2 (2014). Preprint at <http://arxiv.org/abs/1412.0210v2> (2014).

[35] Y. Zhang, C. He, Z. R. Ye, J. Jiang, F. Chen, M. Xu, Q. Q. Ge, B. P. Xie, J. Wei, M. Aeschlimann, X. Y. Cui, M. Shi, J. P. Hu, and D. L. Feng, Symmetry breaking via orbital-dependent reconstruction of electronic structure in detwinned NaFeAs. Phys. Rev. B **85**, 085121 (2012).

[36] S-H. Baek, D. V. Efremov, J. M. Ok, J. S. Kim, Jeroen van den Brink and B. Büchner, Orbital-driven nematicity in FeSe. Nat. Mater. **14**, 210-214 (2015).

[37] T. Shimojima, Y. Suzuki, T. Sonobe, A. Nakamura, M. Sakano, J. Omachi, K. Yoshioka, M. Kuwata-Gonokami, K. Ono, H. Kumigashira, A. E. Böhmer, F. Hardy, T. Wolf, C. Meingast, H. v. Lühneysen, H. Ikeda, K. Ishizaka, Lifting of *xz*/*yz* orbital degeneracy at the structural transition in detwinned FeSe. Phys. Rev. B **90**, 121111 (2014).

[38] M. D. Watson, T. K. Kim, A. A. Haghighirad, N. R. Davies, A. McCollam, A. Narayanan, S. F. Blake, Y. L. Chen, S. Ghannadzadeh, A. J. Schofield, M. Hoesch, C. Meingast, T. Wolf, A. I. Coldea, Emergence of the nematic electronic state in FeSe. Phys. Rev. B **91**, 155106 (2015).

[39] A. E. Böhmer, T. Arai, F. Hardy, T. Hattori, T. Iye, T. Wolf, H. v. Löhneysen, K. Ishida, and C. Meingast, Origin of the tetragonal-to-orthorhombic phase transition in FeSe: a combined thermodynamic and NMR study. Phys. Rev. Lett. **114**, 027001 (2015).

[40] Q. Wang, Y. Shen, B. Pan, Y. Hao, M. Ma, F. Zhou, P. Steffens, K. Schmalzl, T. R. Forrest, M. Abdel-Hafiez, D. A. Chareev, A. N. Vasiliev, P. Bourges, Y. Sidis, H. Cao, J. Zhao, Strong Interplay between Stripe Spin Fluctuations, Nematicity and Superconductivity in FeSe. arXiv:1502.07544v1

(2015). Preprint at <http://arxiv.org/abs/1502.07544v1> (2015).

[41] R. M. Fernandes, L. H. VanBebber, S. Bhattacharya, P. Chandra, V. Keppens, D. Mandrus, M. A. McGuire, B. C. Sales, A. S. Sefat, and J. Schmalian, Effects of Nematic Fluctuations on the Elastic Properties of Iron Arsenide Superconductors. Phys. Rev. Lett. **105**, 157003 (2010).

[42] A. E. Bömer, P. Burger, F. Hardy, T. Wolf, P. Schweiss, R. Fromknecht, M. Reinecker, W. Schranz, and C. Meingast, Nematic Susceptibility of Hole-Doped and Electron-Doped $BaFe_2As_2$ Iron-Based Superconductors from Shear Modulus Measurements, Phys. Rev. Lett. **112**, 047001 (2014).